Remote detection of stress corrosion cracking: Surface composition and crack detection

Cliff J. Lissenden, Igor Jovanovic, Arthur T. Motta, Xuan Xiao, Samuel Le Berre, David Fobar, Hwanjeong Cho, and Sungho Choi

Citation: AIP Conference Proceedings **1949**, 110003 (2018); doi: 10.1063/1.5031582
View online: https://doi.org/10.1063/1.5031582
View Table of Contents: http://aip.scitation.org/toc/apc/1949/1
Published by the American Institute of Physics

Remote Detection of Stress Corrosion Cracking: Surface Composition and Crack Detection

Cliff J. Lissenden[1a], Igor Jovanovic[3], Arthur T. Motta[2], Xuan Xiao[2], Samuel Le Berre[2], David Fobar[3], Hwanjeong Cho[1], Sungho Choi[1]

[1]*Department of Engineering Science and Mechanics, Pennsylvania State University, University Park, Pennsylvania, USA*
[2]*Department of Mechanical and Nuclear Engineering, Pennsylvania State University, University Park, Pennsylvania, USA*
[3]*Department of Nuclear Engineering and Radiological Sciences, University of Michigan, Ann Arbor, Michigan, USA*

[a)]Corresponding author: lissenden@psu.edu

Abstract. Chloride induced stress corrosion cracking (SCC) of austenitic stainless steel is a potential issue in long term dry storage of spent nuclear fuel canisters. In order for SCC to occur there must be a corrosive environment, a susceptible material, and a driving force. Because it is likely that the material in the heat affected zone (HAZ) of welded stainless steel structures has been sensitized as a result of chromium depletion at the grain boundaries and a thermal residual stress driving force is likely present if solution annealing is not performed, two issues are critical. Is the environment corrosive, i.e., are chlorides present in solution on the surface? And then, are there cracks that could propagate? Remote detection of chlorides on the surface can be accomplished by laser induced breakdown spectroscopy (LIBS), while cracks can be detected by shear horizontal guided waves generated by electromagnetic acoustic transducers (EMATs). Both are noncontact methods that are amenable to robotic delivery systems and harsh environments. The sensitivity to chlorine on stainless steel of a LIBS system that employs optical fiber for pulse delivery is demonstrated. Likewise, the ability of the EMAT system to detect cracks of a prescribed size and orientation is shown. These results show the potential for remote detection of Cl and cracks in dry storage spent fuel canisters.

INTRODUCTION

Management of the nuclear fuel cycle is an important element of energy production and stewardship of our environment for today and future generations. Issues related to nondestructive evaluation of dry storage casks for spent nuclear fuel have been described elsewhere by the authors [1] and in numerous reports [e.g., 2-5]. Spent nuclear fuel goes to wet storage and then dry storage prior to disposal. Dry storage casks consist of a metal and concrete overpack that protects and provides ventilation for the welded stainless steel canister, which contains the spent fuel assemblies. Stress corrosion cracking (SCC) is a potential mode of degradation in the austenitic stainless steel canisters, and aging management plans are being developed to ensure the structural integrity of the canisters. Atmospheric chloride-induced SCC requires a tensile driving force, a susceptible material, and chlorides in solution on the surface. The welds used to fabricate the storage canisters sensitize the material in the heat affected zone and result in tensile thermal residual stresses. Schematics showing the geometry and fabrication welds of a vertical axis dry storage cask are provided in Fig. 1. Here, we report on the development of sensing capabilities for a robotic inspection system that can detect deposited Cl and the presence of cracks. We describe a laser induced breakdown spectroscopy (LIBS) system to characterize the salt content on the canister surface and an ultrasonic guided wave based crack detection system.

Before describing the LIBS and guided wave sensing capabilities, we highlight features of the robotic inspection system, which has been dubbed PRINSE, for Proactive Robotic Inspection of Nuclear Storage Enclosures.

44th Annual Review of Progress in Quantitative Nondestructive Evaluation, Volume 37
AIP Conf. Proc. 1949, 110003-1–110003-10; https://doi.org/10.1063/1.5031582
Published by AIP Publishing. 978-0-7354-1644-4/$30.00

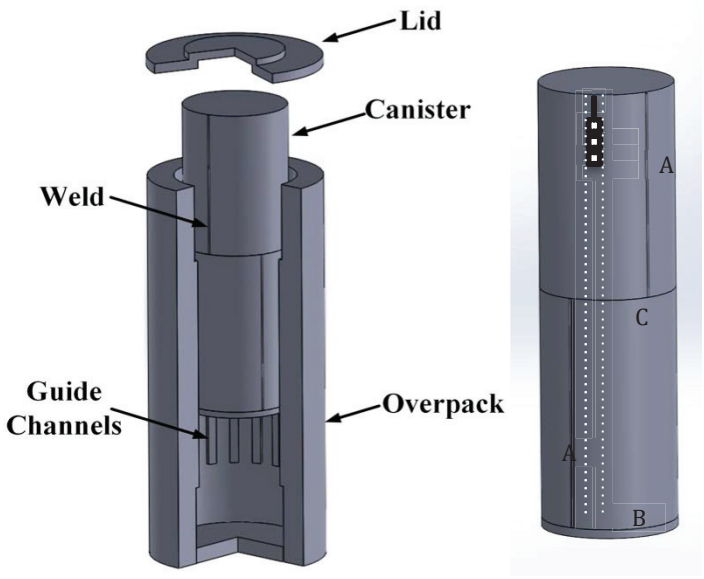

FIGURE 1. Cut-away view of a dry storage cask (left), weld pattern in stainless steel canister (right, A = axial, B = bottom, C = circumferential).

THE PRINSE SYSTEM

The proactive robotic inspection of nuclear storage enclosures (PRINSE) system can be thought of as three-in-one: delivery system, inspection system, and control/data management system. These three features are briefly introduced in this section.

Delivery System

Vertical axis canisters have inlet vents at the bottom and outlet vents at the top. The delivery system consists of:

- a vent mount that is inserted into an outlet vent;
- a flexible delivery arm having a pivot point that is manually slid onto the canister lid through an outlet vent;
- a garage mounted on the delivery arm for parking a sensor train;
- a sensor train of three cars that are launched from the garage over the edge of the canister lid; and
- a winch outside the cask that is connected to the vent mount.

The sensor train delivers the sensor systems to positions on the outside of the canister where measurements are made. In fact, the winch lowers the sensor train to the bottom of the canister so that inspections are made while the sensor train is being raised back up. The first guiding principle for the design of the delivery system is to keep as much of the electronics outside the cask as possible due to the harsh environment (high temperature and gamma radiation). Other guiding principles are to not permit the delivery system to get wedged or jammed inside the cask and to not leave marks on the canister or leave robot components behind. The tight clearance around the canister and the presence of guide channels that keep the canister concentric with the cask limit the size and maneuvering options for the delivery system. In the casks with the most constricted geometry, the sensor train can move only vertically between guide channels.

Inspection System

Four types of measurements are provided by the inspection system: crack detection, surface composition, surface temperature, and radiation dose. In reverse order, radiation dose is measured with a miniature Geiger-Mueller tube to track the PRINSE system components' dose to help manage part replacement, and to calibrate models. The canister surface temperature is measured to help validate canister thermal calculations. High quality measurements of surface temperatures by a Type K thermocouple can help meet this need. Surface composition measurements, with special attention to chloride concentration, can provide an indication of whether chloride induced SCC is possible. A LIBS system provides surface composition characterization and is described subsequently. Finally,

stress corrosion cracks are detected using an ultrasonic guided wave methodology, also detailed below. Of these four measurements only the thermocouple requires contact with the canister. These noncontact measurements are well-suited for robotic inspection.

Control/Data Management System

The PRINSE system is to be controlled from a command center on the concrete pad outside of the cask, and data is acquired and managed from there. The command center will have separate computer controls for the robot, LIBS, and crack detection systems, data storage, and an Ethernet switch. There will also be a vent interface (physically supported by the vent mount) that contains an Ethernet switch, USB hub, a BeagleBone board, and a custom board. At this point, each system is controlled separately, but we envision that all of the controllers could be integrated into one system in future work. Each inspection system will have the capability to provide results in real time, which means that meta data, measured data, and signal processing results will all need to be effectively managed and that the operator will be able to make decisions to acquire more data, move to a different position, or change the planned data acquisition based on findings.

LASER INDUCED BREAKDOWN SPECTROSCOPY

LIBS, a type of optical emission spectroscopy, is based on focusing high-power laser pulses onto the sample surface to generate luminous plasma that contains ionized and excited particles, and resolving the characteristic emissions from the plasma that are unique to specific elements, molecules, or even isotopes. The ability to carry out remote, *in-situ* measurement is one of the major advantages of LIBS, enabling its development in settings that are inaccessible or adverse to human health, especially when LIBS can be delivered via flexible fiber optics. One such opportunity for LIBS is the measurement of chlorine concentrations on stainless steel surfaces within dry cask storage systems. However, the high excitation energy of Cl of over 10 eV makes its direct detection difficult in a fiber delivery configuration, mainly due to the limited laser irradiance that could be obtained on the sample surfaces. Although a recent publication [6] by Eto *et al.* demonstrated the possibility of observing Cl emission in fiber-optic LIBS, reliable detection of the Cl emission line at 837.6 nm remains challenging when quantitative measurements of Cl are sought at low concentrations. Accordingly, a double pulse (DP) excitation technique, designed to separately optimize the processes of laser ablation and plasma excitation, was adopted in our experiments to improve the analytical performance of fiber-optic LIBS in characterization of Cl content on stainless steel surfaces, targeting Cl concentrations in the range of 1-100 mg/m^2.

Figure 2 shows the laboratory setup of fiber-optic LIBS in the collinear DP configuration. A Q-switched Nd: YAG laser (Quanta-Ray PRO-250-10, Spectra Physics) with pulse duration of ~10 ns and a repetition rate of 10 Hz was operated at its fundamental wavelength of 1064 nm. A pulse sequence formed by two pulse replicas with a time separation of 40 ns was generated by splitting the laser beam into two paths using a combination of beam splitters and wave plates, and extending one of the paths to ~12 m to achieve a fixed time delay with respect to the other path. The DP sequence was coupled into a 10-m long, 1-mm core diameter optical fiber using a 300-mm focal length lens, and was collimated and focused onto the sample surface by two tight-focusing lenses with a focal length of 30 mm. The emission light from the plasma was collected in standard atmospheric conditions and diverted through a separate optical fiber into a Czerny-Turner spectrometer (Jobin Yvon iHR550, Horiba) and an ICCD camera (iStar 334T, Andor). A long-pass filter with a cutoff wavelength at 550 ns helped eliminate the second-order diffraction of the iron lines in the region near 400 nm. The timing between the mechanical shutter and the ICCD camera, as well as the gating of the camera were fully controlled by the Solis S acquisition software from Andor. The translation stage provides precise motion control of the sample position during data acquisition.

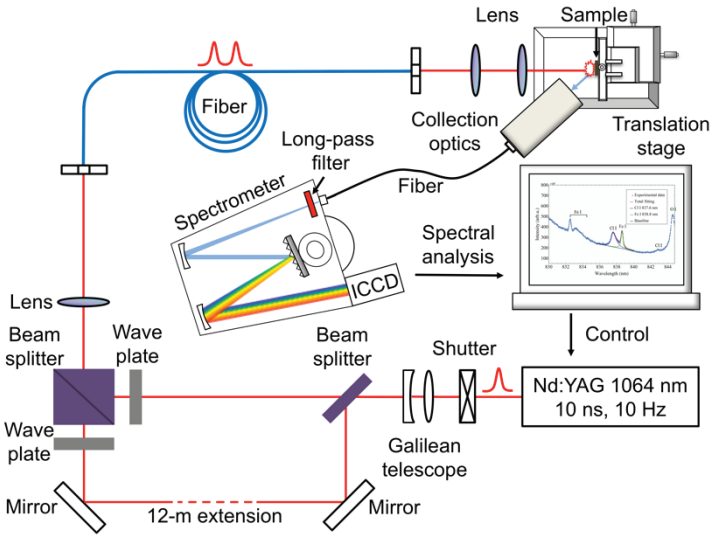

FIGURE 2. Laboratory setup for DP fiber-optic LIBS.

The laser spots obtained in fiber-optic LIBS can be seen in the SEM image shown in Fig. 3. Since different guided modes inside the multimode fiber may interfere with each other, speckle patterns can be observed in the laser spots on the sample surface. The irradiance of the laser pulse was significantly lower when compared to open-beam configuration due to the limited laser energy that could be transmitted via the optical fiber and the poor focus-ability of the highly divergent output beam from the optical fiber. Consequently, the thermal gradient introduced by the laser shot on the sample surface was reduced correspondingly, and as a result, no surface structures (such as a large thermally affected area seen in early observations with open-beam delivery [7]), appeared in the vicinity of the focal spot. This also reduces the risk of thermal alteration of the material microstructure and of introducing thermal stresses.

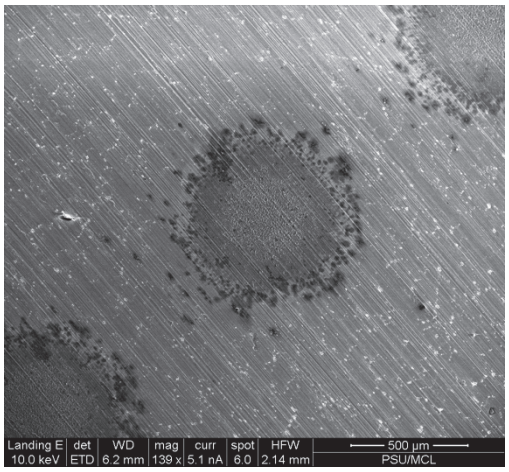

FIGURE 3. SEM image of laser spot in fiber-optic LIBS (FESEM: NanoSEM 630).

To benchmark the LIBS measurement, standard samples with well-known Cl surface concentrations were prepared by a nebulizer-based process [7]. A PerkinElmer Mira-mist nebulizer (P/N N0775330) was used to create fine aerosol particles from the interaction between the synthetic seawater solution (ASTM D1141-98, Lake Products Company LLC) and the argon gas stream. The sea salt aerosol particles were deposited on stainless steel substrates, which were preheated to 500 °C using a hot plate. This resulted in more homogeneous salt depositions relative to the unheated case, with no aggregation and crystallization of salt aerosols observed on the sample surfaces using scanning electron microscopy (SEM), even at high magnification. The surface concentrations of Cl were calculated from the deposition parameters, including the mass concentration of Cl in the diluted seawater solution, the flow rate

of nebulizer, the exposure time of the samples, and the sprayed area. Energy-dispersive X-ray spectroscopy (EDS) and ion chromatography (IC) techniques were used to confirm the distribution and the absolute concentration of Cl on the steel substrates [7]. A set of samples with Cl concentration in the range of 5-100 mg/m^2 were prepared in such a fashion for LIBS calibration.

Figure 4a shows the averaged emission spectra obtained using fiber-optic LIBS over 5 different locations on the sample with single laser burst ablation at each spot. The gate delay, gate width, and gain of the ICCD detector were set at 0.1, 15, and 1000 μs, respectively. The input laser energy was ~37 mJ per pulse, but only ~20 mJ per pulse could be delivered onto the sample surface for LIBS measurement. As can be seen in the spectra, the most intense Cl I emission line (837.6 nm) from the 4p $^4D^o \rightarrow$ 4s ^4P transition of Cl atoms grows and broadens as the Cl concentration increases from 5 mg/m^2 to 100 mg/m^2, whereas the iron (Fe) lines from the matrix do not show appreciable increase. Multiple peak fitting was performed in the spectral area where the Cl I line at 837.6 nm and the Fe I line at 838.8 nm are located. A pseudo-Voigt function was used in the fitting to account for peak broadening. Due to the asymmetric line shape of the Cl I emission, a sigmoidally varied line width was also adopted in the fitting model. The baseline was simply defined as a line joining the data point at the wavelength of 835.6 nm and 840 nm. This nonlinear least square fitting was conducted using the Levenberg-Marquardt algorithm provided in the Mathematica framework.

The peak area intensity of the Cl I line at 837.6 nm was plotted in Fig. 4b versus the calculated Cl surface concentration of the samples. The mean value of the Cl intensity was fitted using a linear dependence on the calculated Cl concentration. The linear fit was shown as solid line in Fig. 4b. The standard deviation of Cl intensity is shown as vertical error bars, while the horizontal ones are the result of an approximate 3-s timing uncertainty in the solution deposition during sample preparation. The coefficient of determination of the linear fitting was found to be 0.87, suggesting that the DP excitation technique can improve the sensitivity of fiber-optic LIBS for direct Cl measurement in the concentration range of 5-100 mg/m^2.

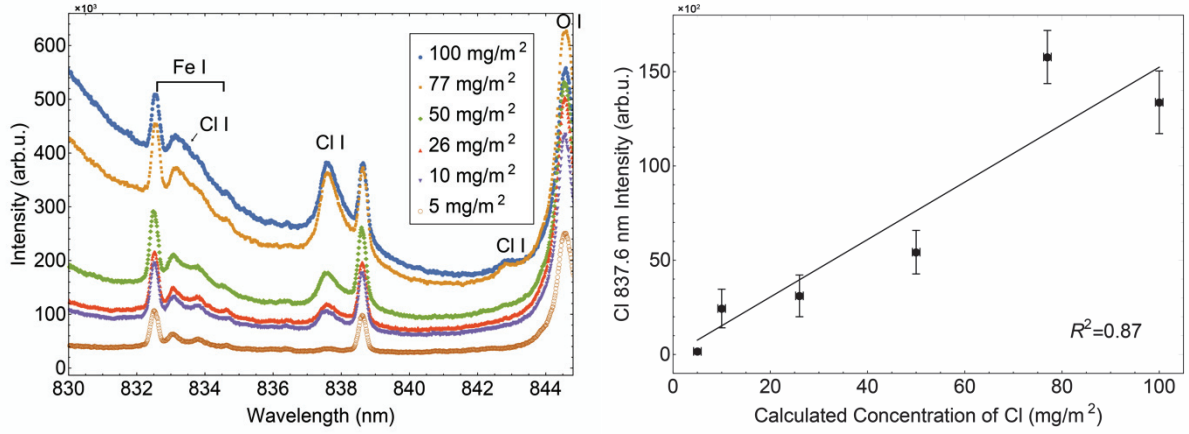

(a) (b)

FIGURE 4. (a) Emission spectra of samples with Cl concentration in the range of 5-100 mg/m^2, (b) Dependence of the Cl I (837.6 nm) emission intensity on the calculated Cl concentration.

Since the focusing lenses and the collection optics developed for the laboratory setup (Fig. 2) cannot be integrated into the sensor train of the PRINSE system for field deployment, a remote optics setup that is tightly assembled into a 3D-printed optical holder was developed specifically for mounting in the sensor train car. Figure 5 shows the assembly of the remote optics, which employs two separate fibers for laser pulse delivery and plasma emission collection. The laser pulses, represented by the red beam in Fig. 5a, were collimated and focused by a 20-mm lens, and diverted in the z direction vertically onto the sample surface. The parabolic mirror collimated the plasma emissions (the blue beam) at an angle of 60° with respect to the incident laser beam. A 30-mm lens focused the emissions back to the fiber for spectral analysis. When connected to fibers, only the remote optics assembly will be carried by a sensor car and inserted into the dry storage cask. The other parts of the LIBS system will be kept at the command center outside the cask.

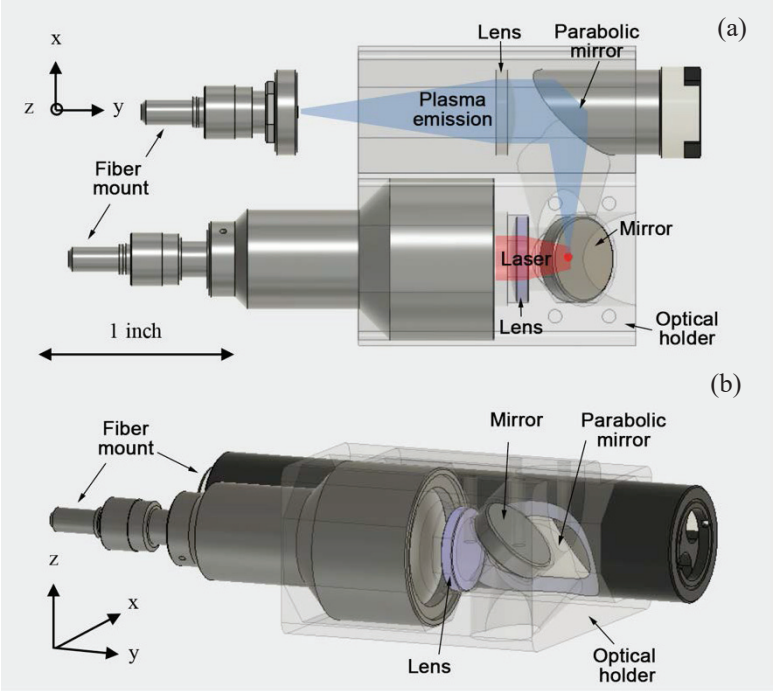

FIGURE 5. Remote optics assembly of robotic delivery car: (a) top view; (b) 3D view.

In the most recent experiments, a compact and portable Q-switched DP Nd:YAG laser (Evergreen 70, Quantel), which is able to provide adjustable inter-pulse delay, was adopted in the fieldable setup of the fiber-optic LIBS system, such that an additional improvement of the sensitivity can be envisioned as we optimize the inter-pulse delay to be on the order of a microsecond [10]. The DP laser, also operated at its fundamental wavelength of 1064 nm, features a pulse duration of ~10 ns at a repetition rate of 10 Hz. Figure 6 gives the preliminary results obtained at inter-pulse delay of 900 ns. The gate delay, gate width, and gain of the ICCD camera were 1200 ns, 300 ns, and 2500, respectively. A clear emission signal characteristic for Cl can be observed in the spectra of sample with a Cl concentration as low as 10 mg/m^2, which is well separated from the nearby Fe I line. Although a more reliable statistic is needed for Cl measurement in the fieldable setup, it can already be seen that the fiber-optic LIBS system can achieve sufficient sensitivity in this application with the assistance of DP excitation technique, and further improvements are possible to obtain a limit of detection better than ~10 mg/m^2.

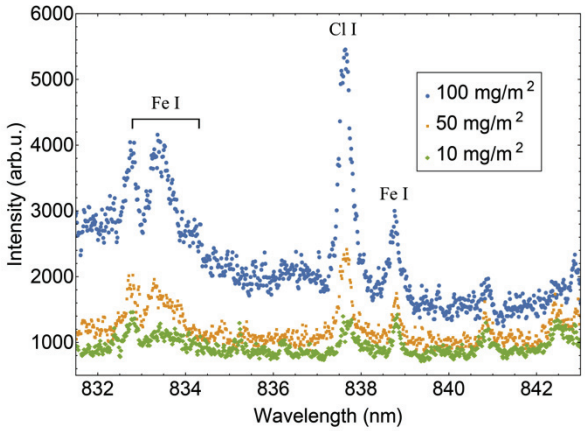

FIGURE 6. Emission spectra of samples with Cl concentration in the range of 10-100 mg/m^2; spectra obtained in the fieldable setup with DP Nd: YAG laser and remote optics assembly.

ULTRASONIC GUIDED WAVES

Ultrasonic guided waves interact with defects like cracks through scattering and reflection and therefore are useful for crack detection. The guided waves are actuated and received by transducers delivered by the sensor train. The sensor train is restricted to move vertically in the gaps between guide channels. The axial welds (shown in Fig. 1) could be completely hidden behind guide channels depending on how the canister is placed inside the overpack, and the guide channels also obstruct almost 50% of the circumferential weld line. The ability of ultrasonic guided waves to propagate reasonably long distances makes them a great choice to provide full coverage of the weld lines. Noncontact transduction is preferred since the inspection must be performed robotically and dispensing of couplant is undesirable. Finally, the 3D nature of shear horizontal (SH) guided waves enables them to interact with cracks oriented either transverse to the wave vector or parallel to it [9], which is important here because analysis of residual stresses indicates that stress corrosion cracks are most likely to grow either transverse to or along weld lines. Electromagnetic acoustic transducers (EMATs) [10] provide excellent capabilities for the operational inspection situation described above. Thus, a robotic inspection protocol has been developed based on EMATs that transmit and receive SH waves propagating circumferentially around the canister. The pulse-echo mode of inspection is employed, where a sensor car contains one EMAT that actuates SH waves that travel away from the sensor car and one EMAT that receives any SH waves that are reflected or scattered from stress corrosion cracks.

The selection of periodic permanent magnetic EMATS for this application is described by Choi et al. [11], while their development is reported by Cho et al. [12]. This section provides an overview of the methods being developed and a demonstration of capabilities.

Ultrasonic guided waves are dispersive and multimodal in nature; phase and group velocity dispersion curves for SH waves propagating in stainless steel plate are given in Fig. 7. The large radius-to-wall thickness ratio of the canister means that these curves provide a very good approximation for SH wave propagation in the canister. The send/receive EMAT pair is shown in a sensor car in Fig. 8. Separate “send” and “receive” EMATs are used because of ringing in the “send” EMAT during the time when crack reflections would be received. The primary components of the EMAT are an array of rare earth magnets, a flexible printed circuit board, and an aluminum housing. As described by Cho et al. [12], the EMAT materials are compatible with the dry storage cask environment. A 5-cycle tone-burst signal having a central frequency of 250 kHz is generated by a high power gated amplifier (RAM 5000, Ritec) and sent to the “send” EMAT through a matching network and 15 m long coaxial cable. The “receive” EMAT signal is sent through a 15 m long coaxial cable to a matching network, a 40 dB pre-amplifier, a 100-500 kHz bandpass filter, and then an oscilloscope, where the signal is recorded. Only the EMATs and coaxial cable go inside the cask, as the other components are located in the command center outside the cask.

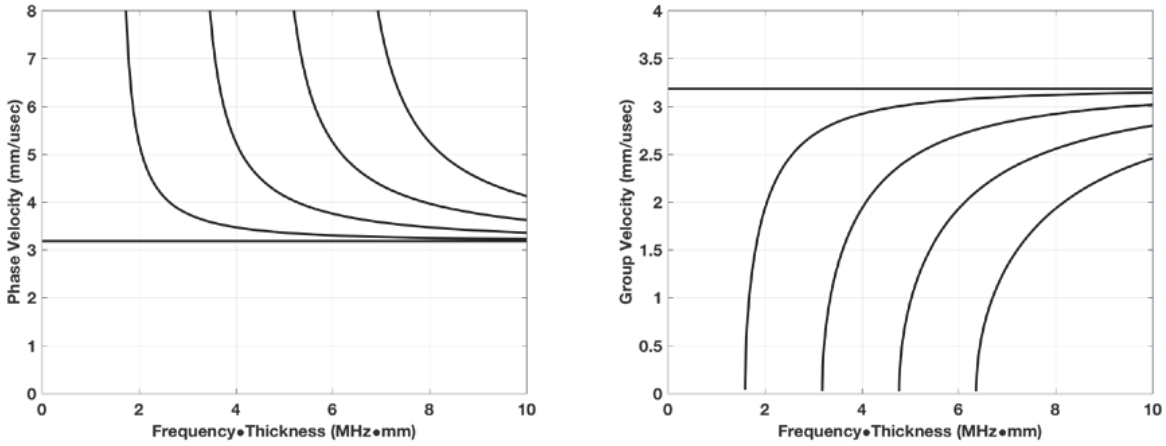

FIGURE 7. Phase velocity and group velocity dispersion curves for stainless steel plate.

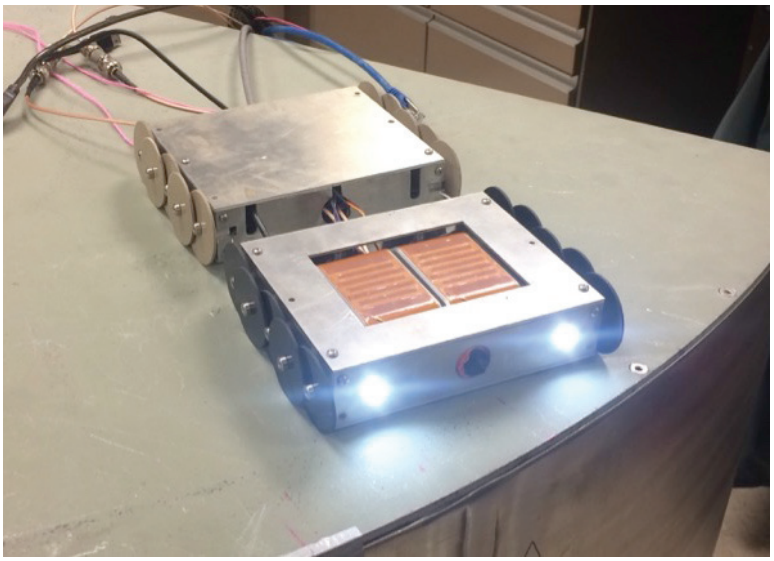

FIGURE 8. EMATs mounted in a sensor car.

The crack detection system targets semicircular cracks having a depth of at least 5 mm. An experiment was devised to determine at what distances from the crack the EMATs could detect it. Two semicircular notches 5.3 mm deep were machined into a 15.9 mm thick 304 stainless plate. The EMAT pair was placed to the right of the notches. One notch is oriented perpendicular to the SH wave vector, while the other is oriented parallel to the SH wave vector. The end wall of the plate is located 203 mm to the left of the notches, which will cause an echo that is the dominant feature in the received signal. The scattering and reflection from the notches will occur significantly earlier than the end wall echo. Based upon the plate thickness there are two propagating modes, SH0 and SH1 having group velocities of 3.2 and 2.9 mm/μs, respectively. The EMAT pair is placed 50.8 mm from the notch and then moved in 6.4 mm increments away from the notch. The experiment is ended when the EMAT pair is 558.8 mm from the notch. The A-scan obtained for each EMAT pair position is compiled into a B-scan image.

The B-scan image obtained from the notch oriented perpendicular to the wave vector is shown in Fig. 9. The initial portion of the signal contains electromagnetic interference, which basically defines the near-field of the transducer. For the smallest distance from the EMAT to the notch, the end wall echo occurs around 170 μs for both the SH0 and SH1 modes due to their similar group velocities. Likewise, for the smallest distance from the EMAT to the notch, the notch echo occurs around 70 μs. For increasing notch distances, the SH0 and SH1 modes interfere both constructively and destructively creating a beats-like phenomenon. The perpendicular notch is clearly detectable at distances from 100-350 mm.

The B-scan image obtained from the notch oriented parallel to the wave vector is shown in Fig. 10. Not surprisingly, the reflection received from notch tip generated diffraction is smaller than the reflection from a perpendicular notch. However it is clearly detectable from 100-200 mm away. In order to provide full coverage of circumferential welds for these minimum size defects the distance needs to be increased to 350 mm. Signal processing techniques are under investigation.

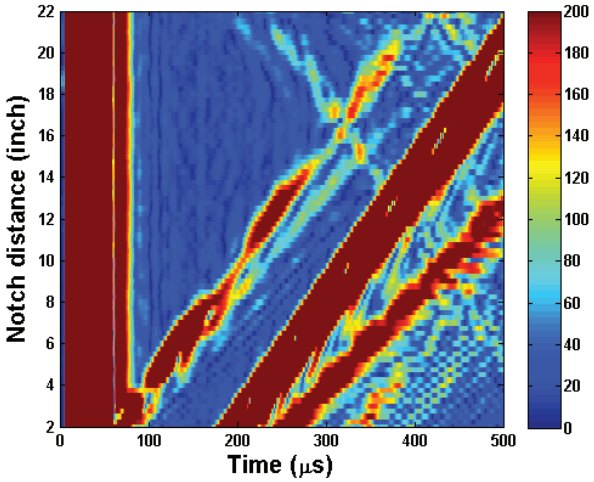

FIGURE 9. B-scan for notch oriented perpendicular to SH wave vector.

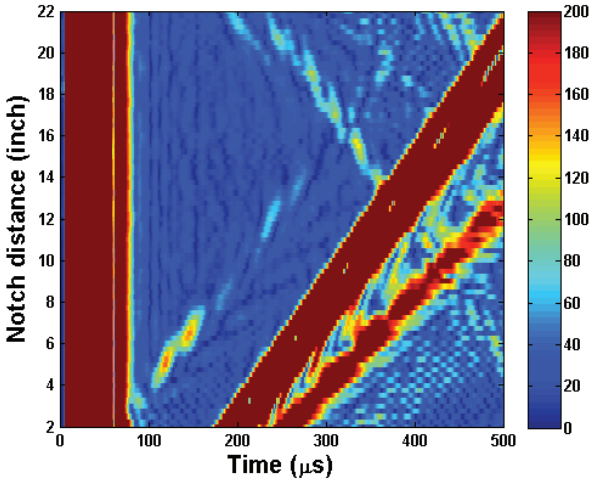

FIGURE 10. B-scan for notch oriented parallel to SH wave vector.

CONCLUSIONS

The Double-pulse (DP) excitation technique has been adopted in a fiber-optic LIBS system for quantification of Cl concentration on stainless steel surfaces, resulting in a significant improvement in detection sensitivity. A compact, fieldable, fiber-optic LIBS seteup that employs a portable DP laser, a 10-m long optical fiber, and a remote optics assembly designed specifically for integration with the robotic sensor car, has been developed and has proved to be effective in detecting of Cl I emissions on samples with Cl surface concentrations as low as ~10 mg/m^2. Even better sensitivity of this fieldable system and more reliable calibration curves at such low Cl surface concentrations can be envisioned in the future as we further optimize the measurement parameters.

A method to detect cracks in the stainless steel canister from a robotic sensor car using noncontact EMATs is also under development. The EMATs send and receive SH waves in the circumferential direction to examine circumferential and axial welds for cracks oriented either transverse or parallel to the weld line using the 3D nature of SH waves. The current capability needs to be enhanced to obtain full coverage of all weld lines for the selected minimum crack size because tip diffraction is not detectable from a sufficiently large setup distance.

ACKNOWLEDGMENTS

We would like to thank Dr. Kyle C. Hartig for his contributions to the LIBS portion of this work and Professors Sean Brennan and Karl Reichard as the leaders of the robotics and system engineering teams. This material is based upon work performed under an Integrated Research Program by the DOE-Nuclear Energy Universities Program under Award number DE-NE0008266.

REFERENCES

1. Lissenden, C.J., Choi, S., Cho, H., Motta, A., Hartig, K., Xiao, X., Le Berre, S., Brennan, S., Reichard, K., Leary, R. McNelly, B., and Jovanovic, I., "Toward robotic inspection of dry storage casks for spent nuclear fuel." *J. Press. Vessel Technol*. **139**:031602, (2017).
2. Chopra, O.K., Dierks, D.R., Fabian, R.R., Han, Z.H., Liu, Y.Y., "Managing aging effects on dry cask storage systems for extended long-term storage and transportation of used fuel," *FCRD-UFD-2014-000476 ANL-13/15*, Argonne National Laboratory, (2013).
3. Meyer, R.M., Pardini, A.F., Cuta, J.M., Adkins, H.E., Casella, A.M., Qiao, A., Larche, M., Diaz, A.A., Doctor, S.R., "NDE to manage atmospheric SCC in canisters for dry storage of spent fuel: an assessment," *PNNL-22495*, Pacific Northwest National Laboratory, (2013).
4. Enos, D.G., Bryan, C.R., Norman K.M., "Data report on corrosion testing of stainless steel SNF storage canisters," *SAND2013-8314P*, Sandia National Laboratory, (2013).
5. Chu, S., "Failure modes and effects analysis (FMEA) of welded stainless steel canisters for dry cask storage systems," *Electric Power Research Institute Report 3002000815*, Palo Alto, California, (2013).
6. Eto S., Fujii T. "Laser-induced breakdown spectroscopy system for remote measurement of salt in a narrow gap, " *Spectrochimica Acta Part B: Atomic Spectroscopy*, **116**: 51-57, (2016).
7. Xiao X., Le Berre S., Hartig K. C., Motta, A.T., and Jovanovic, I. Surrogate measurement of chlorine concentration on steel surfaces by alkali element detection via laser-induced breakdown spectroscopy." *Spectrochimica Acta Part B: Atomic Spectroscopy*, **130**: 67-74, (2017).
8. Babushok V.I., DeLucia F.C., Gottfried J.L., Munson, C.A., and Miziolek, A.W. "Double pulse laser ablation and plasma: Laser induced breakdown spectroscopy signal enhancement." *Spectrochimica Acta Part B: Atomic Spectroscopy*, **61**(9): 999-1014, (2006).
9. Ratassepp, M., Lowe, M.J.S., Cawley, P., Klauson, A., "Scattering of the fundamental shear horizontal mode in a plate when incident at a through crack aligned in the propagation direction of the mode," J. Acoust. Soc. Am. **124**(5): 2873-2882, (2008).
10. Hirao, M., Ogi, H., Electromagnetic Acoustic Transducers, Springer, (2017).
11. S. Choi, H. Cho, C.J. Lissenden, "Selection of shear horizontal wave transducers for robotic nondestructive inspection in harsh environments," *Sensors*, **17**:5, (2017).
12. H. Cho, S. Choi, M.S. Lindsey, C.J. Lissenden, "Electromagnetic acoustic transducer (EMAT) development for nondestructive inspection of spent nuclear fuel storage canisters," *Proceedings of the ASME 2017 Pressure Vessels & Piping Conference*, ASME International, PVP2017-65926, (2017).